AIAA SciTech Forum
6-10 January 2025, Orlando, FL
AIAA SCITECH 2025 Forum

10.2514/6.2025-2127

Development of a *MATLAB* Tool for Thermal and Structural Analysis of Regeneratively Cooled Liquid Rocket Engines

Harry Ford*, Jack Tufft †, Krzysztof Bzdyk‡, and Patrick Harkness§
University of Glasgow, Glasgow, Scotland, G12 8QQ, United Kingdom

Cooling channels are typically incorporated into the walls of the nozzle, throat and chamber of a liquid rocket engine to ensure the structure remains within thermo-mechanical limits. Regenerative cooling is typically achieved using cooling channels of varying geometry across the engine, however modelling the non-linear heat transfer in this system can be difficult.

This paper follows the development of a *MATLAB* program for the purpose of designing cooling channel geometries within regeneratively cooled engines. Specifically, the program includes an evaluation of steady-state regenerative cooling and convective and radiative heat transfer. The program assesses the temperature-dependent stresses exerted on the chamber wall and finds the safety factor of the chamber wall during both hot-fire and pre-combustion. Results are in the process of being validated using alternative design programs and empirically.

This software module is part of the *Open Rocket Combustion Analysis* (*ORCA*) application, created by a researchers at the University of Glasgow. *ORCA* has been developed to be a freely distributed numerical tool designed to generate a contour profile for a rocket nozzle to suit user-defined specifications. This module adds the functionality of designing regeneratively cooled channels to the software.

Nomenclature

A	Area	Pr	Prandtl Number
a	Absorptivity	q	Heat Flux
c	Specific Heat Capacity	Q	Total Heat Flux
$c*$	Characteristic Velocity	Re	Reynolds Number
ch	Channel Height	S_c	Channel Perimeter
cw	Channel Width	r	Recovery Factor
D	Diameter	T	Temperature
d_h	Hydraulic Diameter	t	Thickness
E	Young's Modulus	α_w	Coefficient of Thermal Expansion
e	Emissivity	δ_x	Axial Distance Between Stations
fw	Fin Width	η	Efficiency
h	Heat Transfer Coefficient	γ	Ratio of Specific Heats
k	Thermal Conductivity	μ	Dynamic Viscosity
K	Expansion/Contraction Loss Coefficient	ν	Poisson's Ratio
M	Mach Number	σ	Bartz Correction Factor
$\dot{m}$	Mass Flow Rate	σ_{tt}	Thermal Stress
N_u	Nusselt Number	σ_p	Pressure Stress
P	Pressure	σ_t	Total Stress

*Masters Student, Space and Exploration Technology Group, James Watt North, AIAA Member.
†PhD Candidate, Space and Exploration Technology Group, James Watt North, AIAA Member.
‡PhD., Researcher, Space and Exploration Technology Group, James Watt North, AIAA Member.
§PhD., Professor, Space and Exploration Technology Group, James Watt North, AIAA Member.

I. Introduction

A. Scope

Designing cooling channels for regeneratively cooled liquid rocket engines can be a difficult process, particularly for undergraduate teams and early career researchers. The development of a freely distributed thermal analysis tool that aids cooling channel design can benefit and accelerate the production of regeneratively cooled liquid rocket engines. This paper follows the development of a *MathWorks MATLAB* module that is a component of the *ORCA* software; specifically, the design of cooling channels thermal, and structural analyses. The methodology behind the *MATLAB* code is outlined, followed by a comprehensive case study assessing the capability and accuracy of the program, which is then compared against alternative design tools.

B. Heat Transfer in Liquid Rocket Engines

The main modes of heat transfer within a regeneratively cooled rocket engine are: convection between the hot gas flow and the chamber wall, conduction through the chamber wall, and convection from the chamber wall to the coolant flow. Although radiative heat transfer exists, it typically makes up less than 10% of the total heat flux and is therefore neglected when calculating the hot gas side wall temperatures [1]. Within a rocket engine, the primary heat transfer modes are convective heat transfer from the hot gas to the chamber wall, conduction across the chamber wall, and finally convection from the chamber wall to the coolant flow. This process is depicted in Fig. 1.

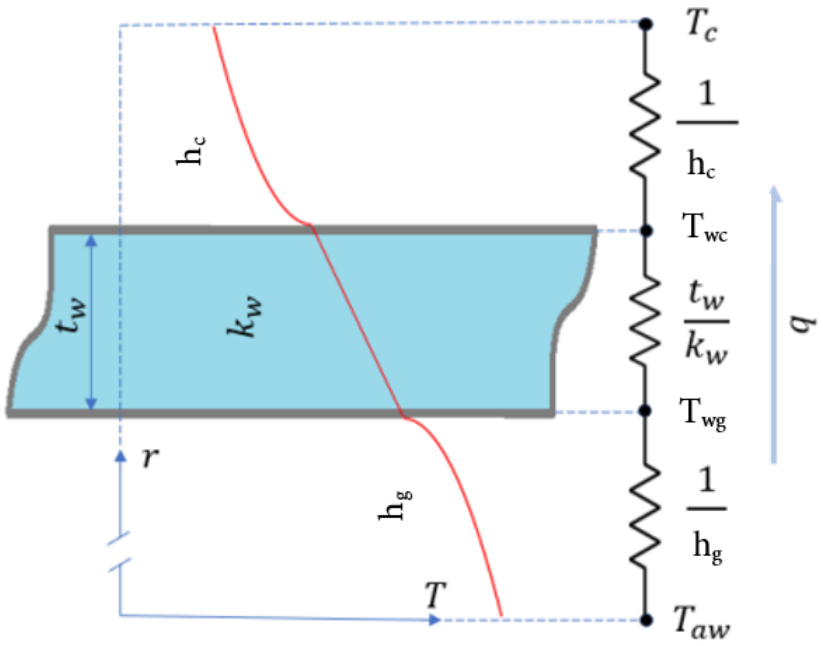

Fig. 1 Diagram of hot gas convection, wall conduction and coolant flow convection heat transfer across the wall of a regeneratively cooled liquid rocket engine. [2]

Using the equations detailed in Fig. 1, equations for the heat fluxes due to convective heat transfer can be found. Eqs. (1) and (2) detail such expressions.

$$q = h_g(T_{aw} - T_{wg}) \tag{1}$$

$$q = h_{c(corrected)}(T_{aw} - T_{wc}) \tag{2}$$

When assuming that the heat transfer acts in a 2D manner, Eq. (3) can be used to compute the heat flux across the chamber wall due to conduction.

$$q = \frac{k_w}{t_w}(T_{aw} - T_{wg}) \tag{3}$$

Equations (1), (2) and (3) can be combined to form Eq. (4) [2].

$$q = \frac{T_{aw} - T_c}{\frac{1}{h_g} + \frac{t_w}{k_w} + \frac{1}{h_{c(corrected)}}} \tag{4}$$

The Bartz equation is a commonly used method for assessing the convective heat transfer from the hot combustion gases to the chamber wall, having been heavily documented, tested and verified in numerous papers [3]. Although radiative heat transfer will exist across the engine, it typically makes up less than 10% of the total heat flux [1], and has hence been assumed negligible when computing wall temperatures. To begin the heat transfer study the Bartz equation, Eq. (5) is firstly computed.

$$h_g = \sigma \left(\frac{0.026}{D_t^{0.2}}\right) \left(\frac{\mu^{0.2} c_{pg}}{Pr_g^{0.6}}\right)_0 \left(\frac{A_t}{A}\right)^{0.9} \left(\frac{P_c}{c^*}\right)^{0.8} \tag{5}$$

Where h_g is the convective heat transfer coefficient from the hot gas flow to the chamber wall, D_t is the diameter of the throat, μ, Pr_g and c_{pg} are the dynamic viscosity, Prandtl number and specific heat at constant pressure of the combustion gases, respectively. A_t is the area of the throat, A is the engine cross-sectional area at the respective station, P_c is the chamber pressure and c^* is the characteristic velocity. σ is a correction factor accounting for property variations within the boundary layer which can be computed using Eq. (6) [4].

$$\sigma = \left[0.5 \left(\frac{T_{wg}}{T_0}\right) \left(1 + \frac{\gamma - 1}{2} M^2\right) + 0.5\right]^{-0.68} \left(1 + \frac{\gamma - 1}{2} M^2\right)^{-0.12} \tag{6}$$

Where T_{wg} is the hot gas-side wall temperature, γ is the ratio of specific heats and M is the local Mach number.

Radiative Heat Transfer exists within a rocket engine due to the emission of electrons and photons from the hot combustion gases. The greater the temperature difference between the combustion gases and the chamber wall, the greater the radiative heat transfer, hence, radiative heat transfer is typically greatest within the combustion chamber [5]. The radiative heat flux within the engine can be found using Eq. (7).

$$q_r = \sigma_{sb} A (\epsilon_g T_g^4 - a_w T_{wg}^4) \tag{7}$$

Where σ_{sb} is the Stefan-Boltzmann constant, A is the chamber wall surface area at the local station, a_w is the absorptivity of the chamber wall and ϵ_g is the emissivity of the combustion gases. As T_{wg} and T_g converge, the absorptivity of the chamber wall approaches that of the emissivity of the hot combustion gases [6].

C. Cooling Methods

1. Regenerative Cooling

Liquid rocket engines typically operate with high combustion temperatures and pressures. To achieve long-duration burns under such conditions, cooling methods must be employed. The most common method of engine cooling is regenerative cooling, implementing cooling channels throughout the structural wall of the engine. Coolant, typically the fuel, flows through the channels and extracts heat from the chamber wall, theoretically allowing for indefinite-duration burns. Cooling channel geometry is typically dictated by the varying heat flux across an engine contour, hence channels are typically at their smallest within the throat region, where heat flux is at a maximum. Once the coolant has passed through the cooling channels, it is injected into the chamber to aid the combustion process itself. Many design considerations must be made to ensure the coolant flow reaches the injector at adequate pressure and temperature, as to avoid propellant backflow and ensure proper propellant mixing.

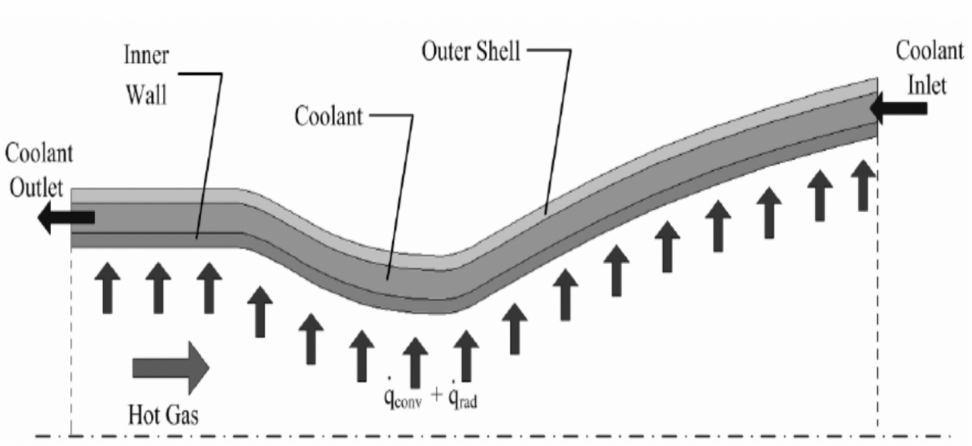

Fig. 2 Cross-section diagram of a cooling channel within a regeneratively cooled liquid rocket engine [7].

2. Film & Transpiration Cooling

Film cooling is another common cooling method. A propellant, typically the fuel, is injected at a disproportionate rate along the chamber wall to develop a boundary layer of fluid, insulating the wall. As the flow travels downstream from the injector and begins to combust, the heavily fuel-rich mixture at the chamber wall will combust at a lower temperature than that of the main propellant mixture in the centre of the chamber. Transpiration cooling involves the fuel flow transpiring from the cooling channels, through the chamber wall, creating a lining on the chamber wall that acts as an insulator, this is not as common as film cooling, likely due to the increased difficulty of manufacture.

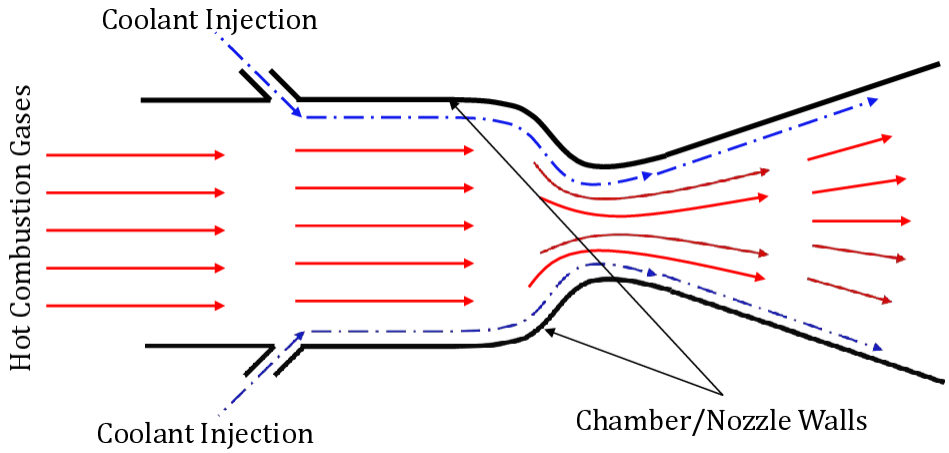

Fig. 3 Diagram of film cooling injection from cooling channels within a rocket engine [8].

3. Ablative Cooling

Ablative cooling typically involves an insulating material being coated onto the chamber wall that is intended to burn up and extract heat as it erodes. Ablatives are normally singular-use, burn-time-limited methods of cooling. They are thus expensive and time-consuming in comparison to methods such as film or regenerative cooling [9]. Ablative liners are commonly a carbon composite-based material, in which the binding polymer melts when heated. As the polymer burns, pyrolysis gases are formed and develop a char layer as they pass through the remaining carbon material [10].

4. Alternative Cooling Methods

Alternative Cooling methods include radiative cooling, in which engines are designed to emit heat via radiation using materials such as Niobium alloys that have very high maximum operating temperatures, up to $1370°C$ [11].

Silicone-based additives are commonly used on small-scale engines; when combusted, they deposit a layer of soot on the chamber wall, acting as a thermal barrier coating. Research at Copenhagen Suborbitals states that diluting the fuel with 1% TEOS (Tetraethyl orthosilicate) can reduce the heat flux to the chamber wall by up to 30% [12]. An alternative paper found that supplementing the fuel with 5% PDMS (Polydimethylsiloxane) can produce heat flux reductions of up to 60% [13]. Working similarly to silicone-based additives, thermal barrier coatings (TBCs) are designed to reduce the heat flux from the hot combustion gases to the chamber wall. TBCs are typically less than 0.5 mm thick and are made up of materials such as Zirconia (ZrO_2) as they have very low thermal conductivity (roughly 1.5 W/(m K)) [14].

D. Manufacturing and Material Choices

1. Chamber Wall Material

Chamber wall material is a crucial design aspect when developing regeneratively cooled liquid rocket engines. The extreme temperatures, pressure, and use of potentially corrosive propellants can inhibit the use of many materials. Commonly used materials for small-scale liquid rocket engines include CuCrZr, AlSi10Mg and Inconel alloys. CuCrZr offers a high thermal conductivity (350 W/(m K)) which can improve the effectiveness of the regenerative cooling design of an engine, however, copper alloys are inherently dense and expensive, reducing its attractiveness as a chamber material. AlSi10Mg is a low-cost option that offers attractive thermal conductivity at the cost of low melt temperatures and structural strength. Inconel is commonly used on rocket engines due to its high strength at high operating temperatures, it does however have a low thermal conductivity in comparison to the aforementioned materials.

2. Additive Manufacturing

The development of powder bed fusion printers in recent years has accelerated the prototyping timeline for small-scale rocket engines significantly. Additive manufacturing particularly suits engines utilising regenerative cooling as the cooling channels themselves can be contained within the chamber wall, allowing the engine to be developed in one manufacturing procedure.

An issue that should be accounted for when designing an engine, intended for being developed using PBF, is the depowdering process. Depowdering, alongside the minimum print dimensions of the PBF printer, are typically the limiting factors on the minimum dimensions of cooling channel geometries. Certain design aspects such as high aspect ratio cooling channels can increase the difficulty of the depowdering process due to the increased surface area to cross-sectional area ratio.

3. Machining and Brazing

Historically, machining and brazing have been the primary manufacturing methods for the development of cooling channels. When machining channels, the desired geometry is typically machined out of a billet of the chamber wall material, leaving the chamber wall and channel fins as the remaining material. The channels are then produced by attaching a closeout, or jacket, directly over the channels using interface bonding methods [15]. These methods include electroplating, or filling the channels with wax, before using electrodeposition to plate the outer surface of the wall with nickel or copper, the assembly is finally heated to remove the wax material [16].

Cooling channels can also be formed by directly brazing thin tubular pipe directly onto the combustion chamber wall, a method primarily known to be used on the F-1 rocket engine used on the Saturn V launch vehicle [17]. Brazing tubes directly onto the combustion chamber is a tedious and time-consuming process that typically requires each cooling channel to be attached by hand. Fig. 4 displays images of chambers with milled channels and brazed tube channels on the left and right, respectively.

(a)

(b)

Fig. 4 Images of (a), cooling channels machined into the chamber wall [18], and (b), brazed channels [19].

E. Thermal Failure Modes of Regeneratively Cooled Liquid Rocket Engines

Several failure modes arise when regenerative cooling is employed, often due to the low wall thickness typically used when designing regeneratively cooled engines.

1. Nucleate Boiling

Nucleate boiling of the coolant flow will occur if T_{wc} exceeds the boiling point of the coolant flow. The process of nucleate boiling can be characterized into different stages, as the presence of nucleate boiling increases. As the temperature of the coolant-side wall increases, the nucleate boiling transitions from free convection, to nucleate, to transition before reaching film boiling. This process is depicted in Fig. 5

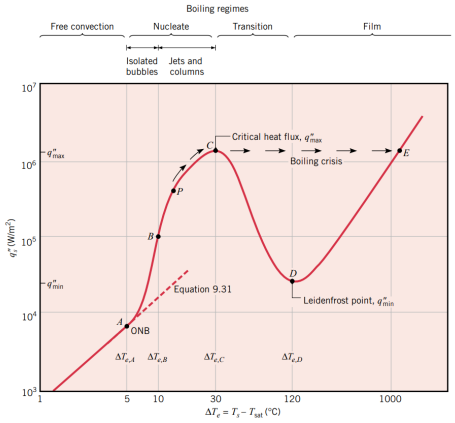

(a)

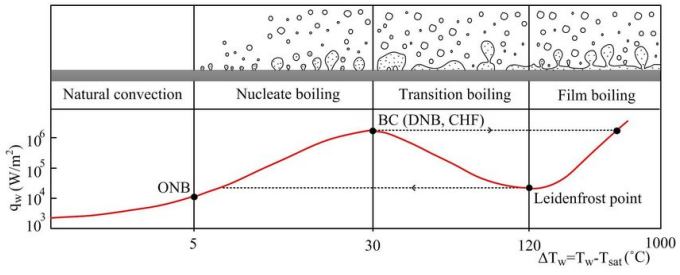

(b)

Fig. 5 Graphs depicting (a), the typical boiling curve for water [20], and (b), a boiling curve illustrating the two-phase flow pattern over a hot plate [21].

Nucleate boiling begins with localised bubbles forming on the surface of the hot plate as it is heated, the point at which these bubbles begin to form is known as the onset of nucleate boiling, (ONB). As the temperature of the hot surface increases, the production of bubbles increases, leading the bubbles to transition to the production of jets and columns. A layer of vapour will eventually be formed across the hot surface, temporarily causing the heat flux to fall due to the lower thermal conductivity of the vapour, this phase is called transition boiling [20]. Once the hot surface is entirely covered by a layer of vapour, the process is said to have reached the Leidenfrost point, at which the heat flux reaches a minimum. As the temperature further increases, film boiling occurs and the heat flux grows.

2. Burn-through and Dog-housing

If the chamber wall fails due to the high temperatures within the combustion chamber, burn-through will occur. Burn-through typically causes the wall between the chamber and the cooling channels to fail and, due to the higher pressure of the coolant flow relative to the chamber flow, coolant will flow directly into the chamber.

The dog-house effect is a common failure mode in regeneratively cooled liquid rocket engines that is induced by repeated hot-firing of the engine. Over time, the fatigue can lead to deformation and thinning of the chamber wall, ultimately, this can cause a burn-through from the cooling channels into the chamber [22]. Figure 6 displays a cross-sectional view of a cooling channel that has undergone dog-housing, with the original cooling channel geometry highlighted.

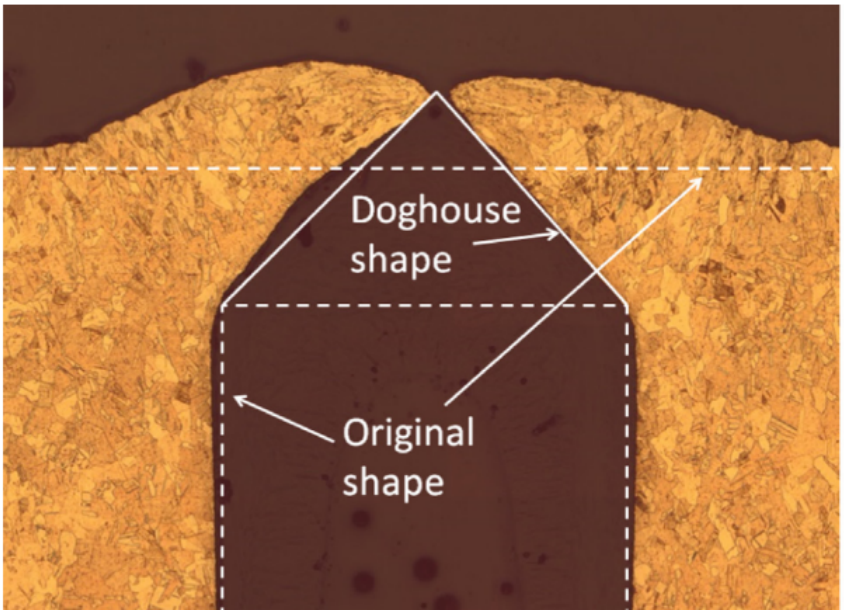

Fig. 6 Cross section view of dog-housing after 48 testing cycles ultimately failing [23].

F. Stresses

The extreme heat produced by a rocket engine will deteriorate the mechanical properties of the chamber wall. *ORCA* intends to assess and analyse the temperature-dependent stress exerted on the chamber wall and subsequently predict the safety factor at each engine station. This assessment can be completed for both combustion and no-combustion scenarios. Longitudinal and tangential thermal stresses and tangential pressure stresses are assessed using the Von-Mises Criterion. Von-Mises is used as although all stresses may independently be below the yield stress, failure may still occur due to the combination of stresses [24]. Safety factor calculations are based upon the Von-Mises stress.

1. Thermal Stresses

Due to the high temperatures, a thermal load is imposed on the chamber wall due to the desire of the heated material to expand. As the chamber wall is a fixed material, it is unable to expand and hence stresses are produced. This process continues until the material reaches the yield point [25]. To minimise the thermal stresses, the wall thickness is ideally

minimised as this will reduce the temperature difference across the chamber wall [26]. As expansion occurs in all directions, the thermal stresses must be considered in both tangential and longitudinal directions.

2. Pressure Stresses

In a regeneratively cooled liquid rocket engine, the pressure in the chamber and cooling channels can be said to counteract each other, as they act upon opposite sides of the chamber wall. As the cooling channel pressure typically exceeds that of the chamber flow, the overall pressure stress on the chamber wall is compressive, acting towards the engine centre-line [27]. A scenario that must be considered is the no combustion case when coolant flow is passing through the cooling channels, yet combustion hasn't yet started. Before combustion, the pressure difference across the chamber wall will be large. For small-scale engines, this is typically of less concern than the combustion scenario; however, if repeated hot-firing is to be completed with the chamber wall remaining at high temperatures, the risk of failure will increase [28] [29].

II. Methodology

As this code is a subset of the *ORCA* program, it is assumed that several parameters such as the engine contour and mass flow rates have been previously calculated and subsequently imported into this module. The heat transfer model features many equations that are dependent on each other, thus requiring iterative loops to converge to final outputs.

A. Engine Stations

To analyse the thermal and structural properties of the engine at different locations along the contour, the engine is split into several locations at which the thermal and structural models will be computed. Each of these locations is labelled as a station. Increasing the number of stations will improve the accuracy of the simulations at the expense of increasing the quantity of data points and time to compute. Due to the iterative process required to solve the thermal analysis, loops are utilised in the *MATLAB* code to converge output values for each parameter. *MATLAB* plug-ins such as *MATLAB CEA* and *CoolProp* allow temperature and pressure-dependent properties of both the chamber and coolant flows to be found, which are incorporated into the iterative loop. The *MATLAB* code handles the current station as station i, with the initial station located at the chamber inlet. In the current state of the *MATLAB* code, the coolant enters at the nozzle end of the engine, thus assumed to be entering at the final station, then flowing opposite to the chamber flow, ultimately reaching the initial station at the chamber inlet before being injected into the chamber itself.

B. Mach Number and Adiabatic Wall Temperature

The first step in the thermal analysis is to predict the Mach number at each engine station. Since the thermal analysis module of the *ORCA* program is completed after the engine contour module, the cross-sectional area at each station is known. Knowing this, the engine is sectioned into subsonic and supersonic regions, and a Mach number of 0.1 is assigned to subsonic regions and 1.5 to supersonic regions. This initial assumption is optimised using an iterative solver that evaluates the cross-sectional area of the station to predict the Mach number at the station.

C. Gas Convective Heat Transfer

The first step in assessing the gas convective heat transfer is to find the adiabatic wall temperature within the engine. The adiabatic wall temperature is the temperature the chamber wall reaches in the case that heat transfer does not exist, and can be computed using Eq. (8) [4].

$$T_{aw} = T_0 \left[\frac{1 + r\left(\frac{\gamma-1}{2}\right) M^2}{1 + \left(\frac{\gamma-1}{2}\right) M^2} \right] \tag{8}$$

Where T_0 is the stagnation temperature of the combustion and r is the recovery factor at the local station, found using Eq. (9) for turbulent flow.

$$r = Pr_g^{0.33} \tag{9}$$

After computing the adiabatic wall temperature, as well as the convective heat transfer coefficient, detailed in Section I.B, the convective heat flux from the hot gas to the chamber wall can be found using Eq. (10).

$$q = h_g(T_{aw} - T_{wg}) \tag{10}$$

D. Coolant Convective Heat Transfer Coefficient

The coolant convective heat transfer coefficient is dependent on the cooling channel geometry, which is a required input by the user for the *ORCA* program. With the user inputs, the channel cross-section area is first found using $A_{channels} = ch \cdot cw$, as is the cooling channel perimeter, $S_c = 2(ch + cw)$. The hydraulic diameter is often found when assessing pipes of non-circular cross-section, which is found using $d_h = \frac{4A_{channels}}{S_C}$. The Reynolds number of the coolant flow must be found, requiring the mass flow rate of the coolant flow through each channel. As both the mass flow rate and the number of channels are directly found from user inputs, the Reynolds number can be found using $Re_c = \frac{4\dot{m}_{channel}}{\pi d_h \mu_c}$. The Nusselt number is also required for the assessment of the coolant convective heat flux, found using $Nu_c = 0.023 Re_c^{0.8} Pr_c^{0.4}$. The Nusselt number is found using the Dittus-Boelter correlation, a simplified method requiring the Reynolds and Prandtl numbers [20]. The heat flux from the chamber wall to the coolant flow is computed using Eq. (11), as described by [2].

$$h_c = \frac{Nu_c k_c}{d_h} \tag{11}$$

Due to a fin effect that arises from direct conduction from the chamber wall through the fin, a correction factor, $m = \sqrt{\frac{2h_c fw}{k_w}}$ is factored into the coolant convective heat transfer coefficient using Eqs. (12) and (13) [2].

$$\eta_f = \frac{tanh\frac{mch}{fw}}{\frac{mch}{fw}} \tag{12}$$

$$h_{c(corrected)} = h_c \left(\frac{cw + 2\eta_f ch}{cw + fw} \right) \tag{13}$$

Knowing the corrected coolant convective heat transfer coefficient, the overall heat flux from the hot gas to the coolant flow can be found using Eq. (4).

E. Temperatures and Coolant Properties

In order to first complete the convective heat transfer detailed in I.B, the gas-side wall temperatures must be known. However, *ORCA* initialises the wall temperatures with an arbitrary array, allowing the heat transfer coefficient to be found. The wall temperatures are then iteratively solved and updated as required until the loop converges. The hot-gas and coolant side wall temperatures can be found using Eqs. (14) and (15) respectively.

$$T_{wg} = T_{aw} - \frac{q}{h_g} \tag{14}$$

$$T_{wc} = T_c + \frac{T_{aw} - T_c}{1 + h_{c(corrected)} \left(\frac{t}{k_w} + \frac{1}{h_g} \right)} \tag{15}$$

When calculating the coolant temperature, reference should be taken to Section II.A, as calculation of the coolant temperature requires iterating upon the data from a previous station, hence, the station notation, i, has been included in Eq. (16).

$$T_{c(i)} = Tc_{(i+1)} + \frac{Q_{w(i)}}{cp_{c(i)} \dot{m}_{coolant}} \tag{16}$$

Once all temperatures have been calculated, the heat transfer study will then assess whether the process has converged, indicating that the code should exit the loop. The newly computed temperatures are used to recalculate the heat flux at each station, allowing the total engine heat flux to be attained. If the magnitude of the differences between subsequent iterations of the total heat flux is less than a convergence tolerance, $\delta_{convergence}$, the code will exit the loop [30].

F. Coolant Properties

The coolant pressure is found using the Darcy friction factor from the Halaand equation. To assess the pressure in the coolant flow, the dimensionless friction factor is found using Eq. (17) [31] [32].

$$\frac{1}{\sqrt{f}} = -1.8log_{10}\left[\frac{6.9}{Re_c} + \left(\frac{\epsilon/d_h}{3.7}\right)^{1.11}\right] \tag{17}$$

With the Darcy friction factor, expansion and contraction loss coefficients as described by [33] are found, Eqs. (18) and (19). These Equations are subsequently used in Eq. (20) to compute the pressure of the coolant flow at each station.

$$K_{(i)} = \left[\left(\frac{d_{h(i)}}{d_{h(i-1)}}\right)^2 - 1\right]^2 \tag{18}$$

$$K_{(i)} = 0.5 - 0.167\frac{d_{h(i-1)}}{d_{h(i)}} - 0.125\left(\frac{d_{h(i-1)}}{d_{h(i)}}\right)^2 - 0.208\left(\frac{d_{h(i-1)}}{d_{h(i)}}\right)^3 \tag{19}$$

$$P_{coolant(i-1)} = P_{coolant(i)} - \frac{\dot{m}^2_{channel} f_{(i)} \delta_x}{(2\rho_{c(i)} d_{h(i)} A^2_{channels(i)})} + K_{(i)} \tag{20}$$

Coolant velocity is found using the volumetric flow rate of the coolant and the cross-sectional area of the channels at each station. Equations (21) and (22) are used to find the coolant velocity at each station.

$$Q_c = \frac{\dot{m}_{coolant}}{\rho_c} \tag{21}$$

$$V_{coolant} = \frac{Q_c}{A_{channels} N_c} \tag{22}$$

ORCA has the ability to produce a plot of the cross-sectional view of the cooling channels at the engine throat, allowing the user to visually assess the channels, walls and fins whilst conducting the thermal analysis. After selecting the desired inputs for the channel geometry, *ORCA* produces the plots seen in Fig. 15.

G. Thermal and Pressure-Induced Stresses

To assess the stresses experienced by the wall, detailed in Section I.F, Eq. (23) can first be used to compute the tangential pressure stresses experienced by the chamber wall [34].

$$\sigma_{tp} = \frac{(P_{coolant} - P_g)}{2}\left(\frac{cw}{t}\right)^2 \tag{23}$$

The thermal stresses in the tangential and longitudinal directions are computed using Eqs. (24) and (25) are used.

$$\sigma_{tt} = \frac{E\alpha_w qt}{2(1-\nu)k_w} \tag{24}$$

$$\sigma_l = E\alpha_w(T_{wg} - T_{wc}) \tag{25}$$

Computing the Von Mises stress is now completed using Eq. (26), which is subsequently used to find the safety factors relating to the temperature-dependent yield and ultimate tensile strengths.

$$\sigma_{vm} = \sqrt{\frac{1}{2}(\sigma_t - \sigma_l)^2 + \sigma_l^2 + \sigma_t^2} \tag{26}$$

Pressure stresses are minimised by maximising the thickness of the chamber wall, however, the opposite is true for the thermal stresses. Figure 16 visualises this limitation, and indicates the acceptable range for a regeneratively cooled engine. Although other factors such as the thermal conductivity of the wall material have a large bearing on the stresses experienced by the engine, the thickness of the chamber wall is a vital design parameter that should be meticulously assessed in conjunction with manufacturing capabilities.

III. Case Study

To assess the accuracy of the *ORCA* heat transfer module, a case study was outlined in which the output data from *ORCA* was compared against professional engine design tool *RPA*, as well as *COMSOL* thermal simulations. The engine design to be assessed across all three studies is outlined in Table 1.

A. *ORCA* Results

The first of the output plots from the heat transfer module of *ORCA* can be seen in Fig. 7, predicting that the maximum wall temperature shall not exceed roughly 620 K.

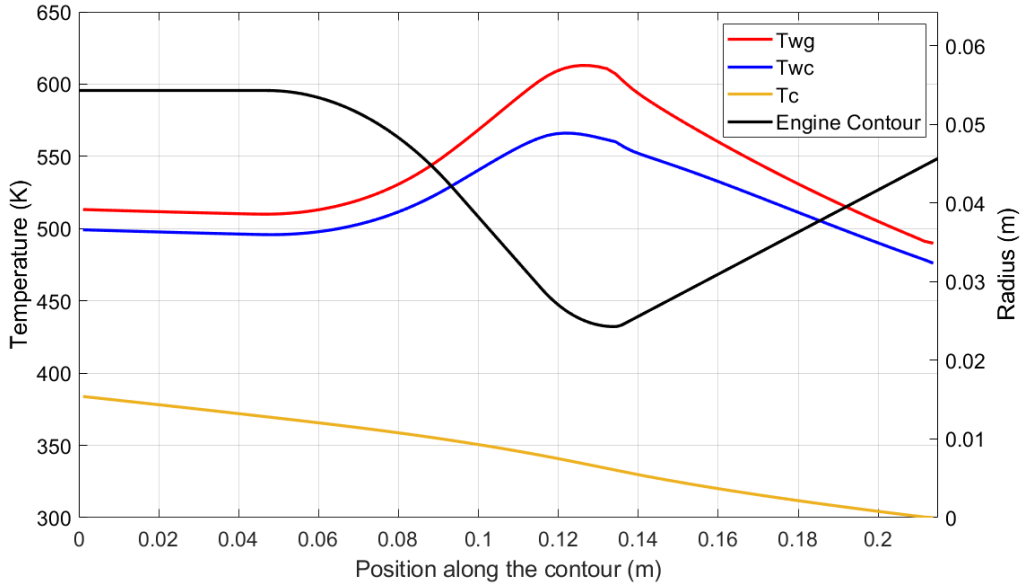

Fig. 7 Wall and coolant temperatures plotted against engine contour

Although the maximum predicted wall temperature of less than 620 K is below the melting point of the AlSi10Mg alloy, stress calculations are completed to ensure that the chamber is not likely to fail. Figure 8 displays the predicted stresses and safety factors the engine shall be subject to during hot-fire.

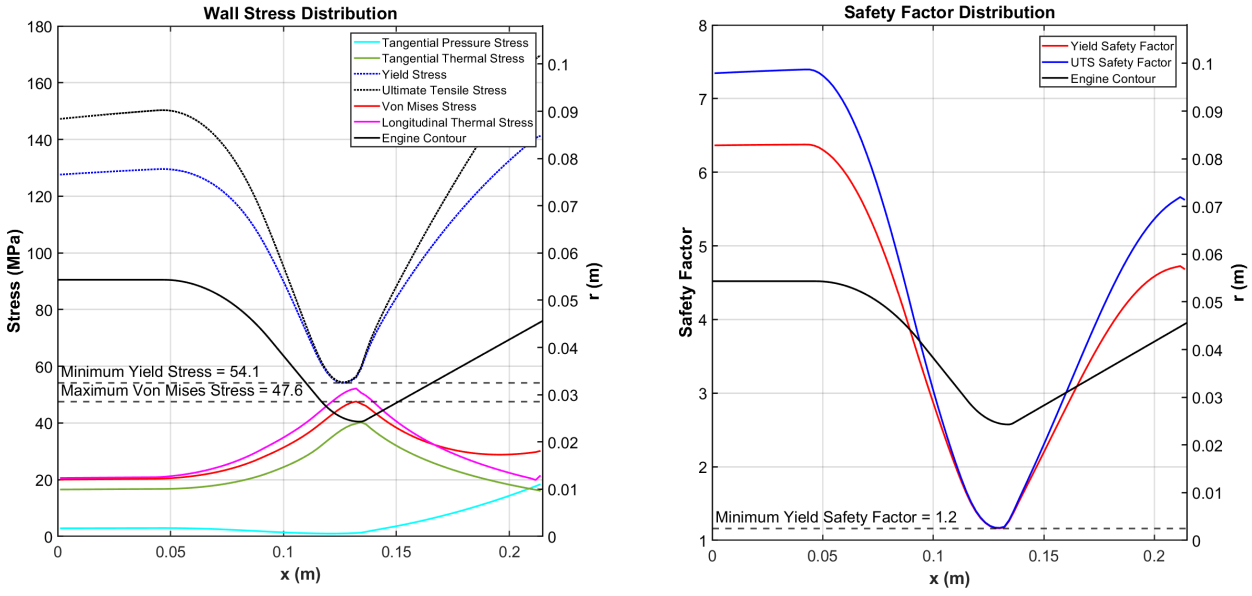

Fig. 8 *ORCA* heat transfer module output graphs for (a), the thermal, pressure, temperature-dependant yield and Von Mises stress, and (b), the yield and ultimate tensile safety factors.

B. Validation

1. RPA Comparison

Rocket Propulsion Analysis (RPA) is a professional rocket design tool that is commonly used in industry. *RPA* is well respected and widely accepted to be accurate to an acceptable level. To assess the accuracy of the *ORCA* thermal analysis, the heat flux and temperature output data was compared to *RPA* and plotted in Fig. 9.

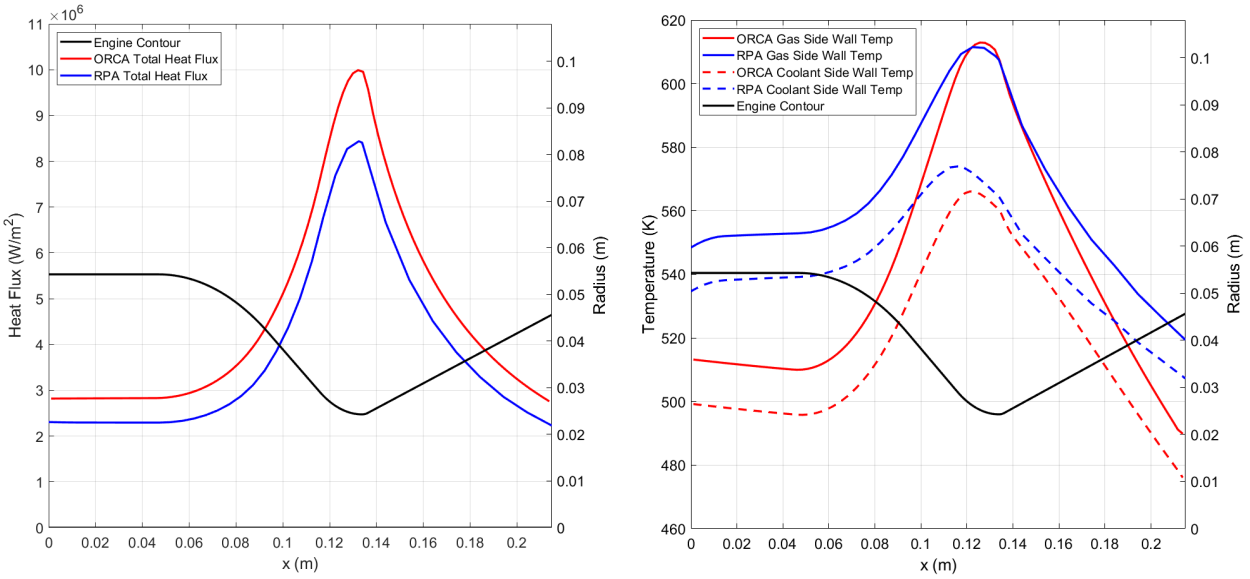

(a) **(b)**

Fig. 9 *ORCA* and *RPA* comparisons of (a), total heat flux from combustion gases to chamber wall, and (b), gas-side and coolant-side wall temperatures.

Figure 9 highlights that *ORCA* predicts slightly higher heat flux across the engine when compared to *RPA*. However, it can also be seen that the maximum predicted wall temperature is within 5 K between *RPA* and *ORCA*. This region of the combustion chamber is at greatest risk of failure when designing a regeneratively cooled engine. *RPA* has also been used to compare the coolant properties to the *ORCA* predictions. Figure 10 displays the comparison plots.

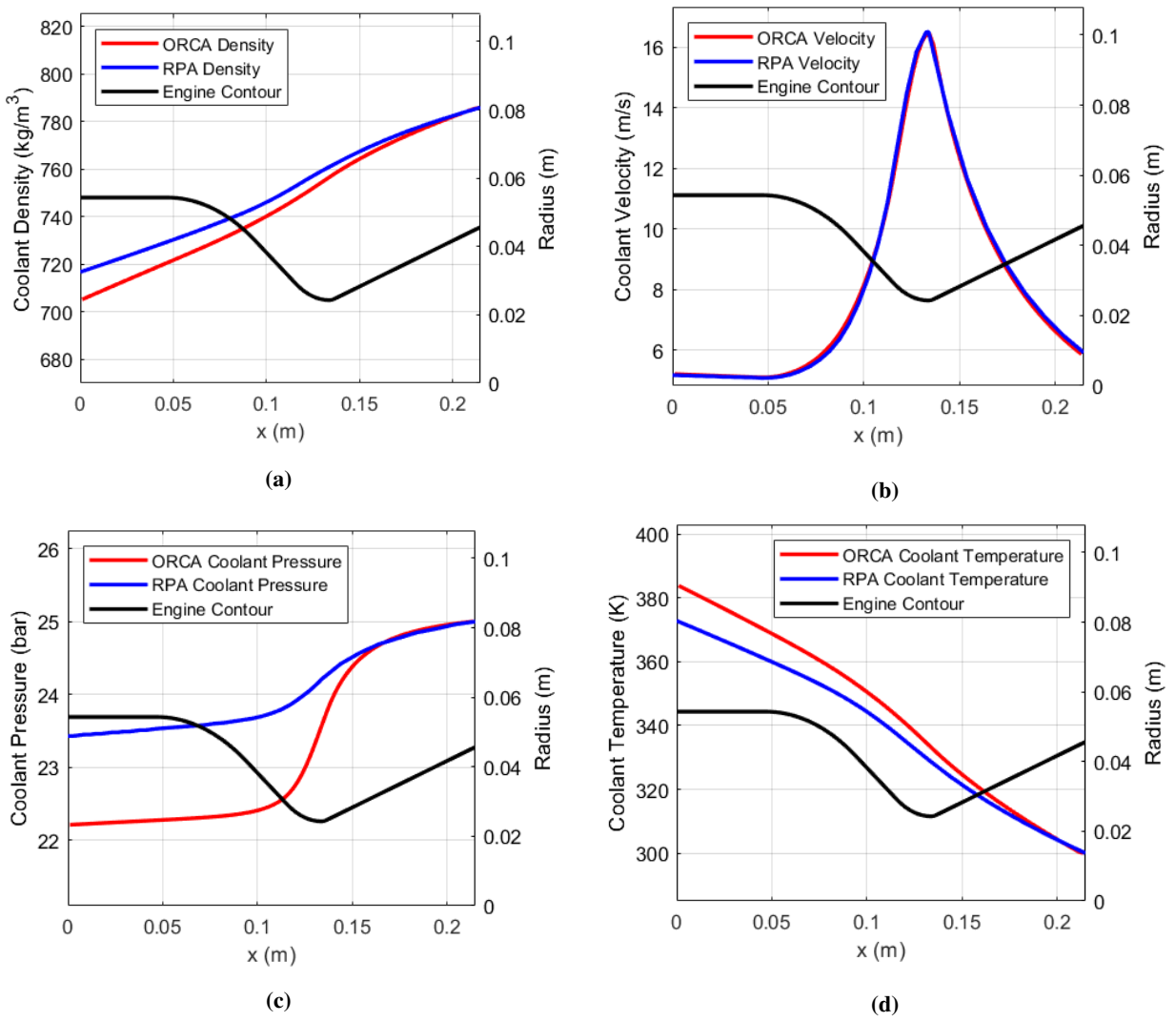

Fig. 10 Comparisons of *ORCA* and *RPA* predictions of coolant (a), density, (b), velocity, (c), pressure and (d), temperature.

2. COMSOL Comparison

COMSOL Multiphysics has been used as a validation method for the *ORCA* heat transfer module. The engine design outlined in Table 1 was modelled and imported into *COMSOL*. Due to the symmetrical nature of each cooling channel, a simulation consisting of one-half of one channel would be sufficient to obtain the necessary data. The output analyses were mirrored and circularly patterned to obtain an analysis of the entire chamber geometry. When setting up the analyses, the convective heat flux coefficient, along with the adiabatic wall temperature, was defined at each of the 100 engine stations. The values for both the convective heat flux coefficient and the adiabatic wall temperature were extracted from the *ORCA MATLAB* module, as the computation methods were derived from basic principles, providing confidence that the numerical values were of suitable accuracy. The finest physics-controlled mesh size 'extremely fine' was applied for both stationary and time-dependent studies. The results of the stationary study can be seen in Fig. 11.

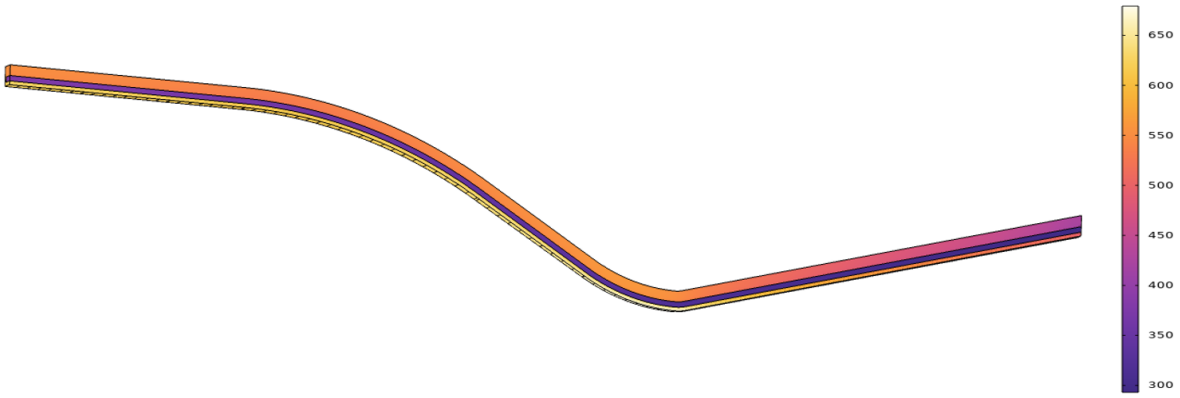

Fig. 11 Thermal analysis of a singular cooling channel using *COMSOL*

A convergence study was completed to ensure that the obtained results were reliable and would not be improved if a finer mesh was applied. Figure 12 details the convergence assessments for the coolant temperature, wall temperature and pressure drop across the cooling channels. It can be seen that from roughly 1,000,000 elements onward, the study can be said to be converged.

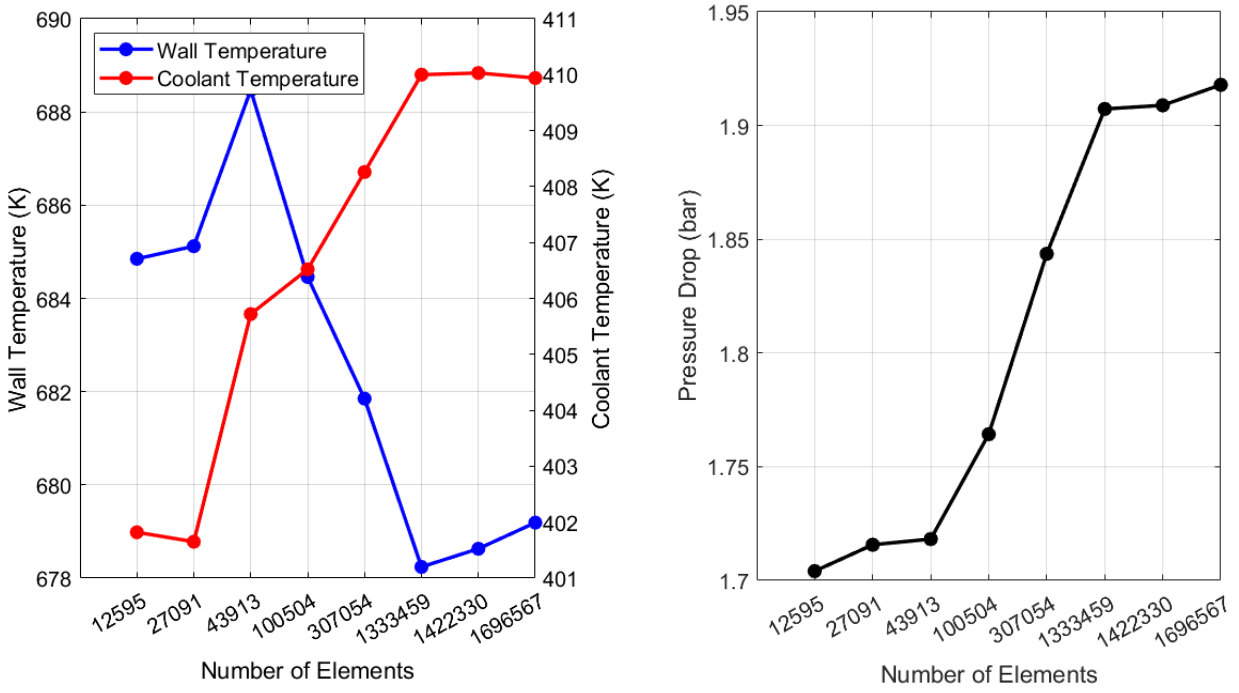

Fig. 12 Convergence analysis plots displaying the convergence of (a), wall and coolant temperature, and (b), coolant pressure drop as the number of elements exceeds 1,000,000.

To assess the accuracy of the *ORCA* heat transfer module in comparison to *COMSOL*, the output data was collated in Fig. 13. *COMSOL* predicts the gas-side wall temperatures in the throat region to be roughly 10% higher than the predictions of both *ORCA* and *RPA*. It is believed that as the Bartz solution method is employed for the thermal assessment in both *ORCA* and *RPA*, this is what leads to the similarities in the wall temperature predictions. Commonly, the Bartz equation has correction factors applied for specific use scenarios, it may be the case that for the engine design specified in Table 1, a correction factor will allow for increased accuracy of the predicted wall temperatures. Features

such as Bartz corrections factors may be implemented into the *ORCA* heat transfer module in future. Fig. 13 displays the predicted coolant side wall temperatures predicted by *COMSOL*, *ORCA* and *RPA*.

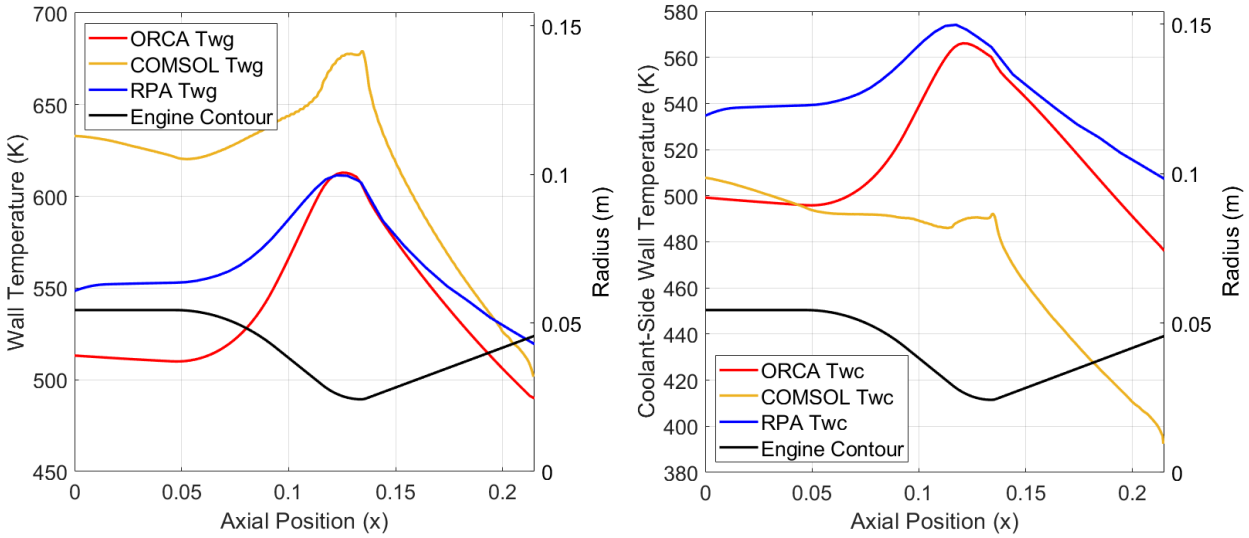

Fig. 13 Comparison of *ORCA*, *COMSOL* and *RPA* predictions of (a), gas-side wall temperature and (b), coolant-side wall temperature

When comparing the *COMSOL* predictions of coolant side wall temperature to that of *ORCA* and *RPA*, the opposite is true for the gas side wall temperature comparison, the *COMSOL* model predicts the wall temperatures to be lower than the predictions of *ORCA* and *RPA*. A key factor in this assessment is the computation of the fin efficiency. When assessing the *COMSOL* model, it was noted that the wall temperature directly below a cooling channel was greater than directly below a fin. This could be due to the high thermal conductivity of AlSi10Mg allowing for greater heat transfer through the wall material than what can be convected to the coolant flow. If there is an inaccuracy in the calculation of the fin efficiency, this will impact the accuracy of the coolant convective heat transfer coefficient, and thus the predicted coolant-side wall temperature. Further investigation will be required to determine the root cause of the difference in predicted coolant-side wall temperatures, and how best to combat any errors with the *ORCA* prediction. The coolant bulk temperature is the next parameter to be compared between the prediction of *ORCA*, *COMSOL* and *RPA*, with the data presented in Fig. 14.

RPA, *COMSOL* and *ORCA* coolant temperature predictions are within 20 K of each other across the engine. The slight increase in predicted coolant temps provided by the *ORCA* heat transfer module, along with the slightly lower predicted gas-side wall temperatures detailed in Fig. 13 suggest that the *ORCA* prediction assumes a greater quantity of heat is being extracted than the alternative methods. Further investigation will be required to assess whether this conception is true. Within the throat region, the rate of temperature increase appears to be at a maximum, which is to be expected given this is the region in which the heat flux is at a maximum.

The final comparison made between the thermal analysis tools is the assessment of the coolant pressure across the engine, Fig. 13 displays that although the *COMSOL* and *RPA* coolant pressure predictions are highly similar, the *ORCA* heat transfer module predicts the coolant to be of lower pressure in the chamber section. Although the discrepancy is less than 5%, or less than 0.2 bar, it is worth investigating further to determine whether an alternative flow pressure calculation method should be employed.

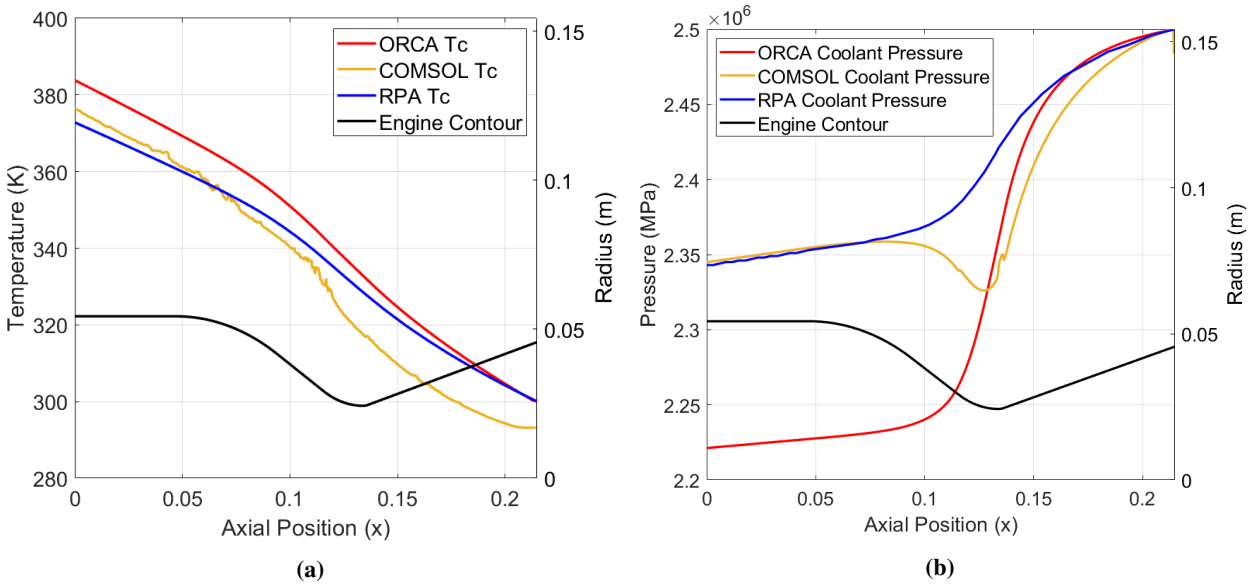

Fig. 14 Comparison of *ORCA*, *COMSOL* and *RPA* predictions for (a), coolant temperature, and (b), coolant pressure.

IV. Conclusion

Due to the difficult nature of developing regeneratively cooled liquid rocket engines, the *ORCA* project was outlined, aimed at lowering the barrier to entry for student teams seeking to develop regeneratively cooled liquid rocket engines. Through the utilization of the Bartz equation, the *ORCA* heat transfer module allows users to assess the impact specific cooling channel designs will have on liquid bi-propellant engine performance. The heat transfer module also includes a structural analysis module that allows users to assess the capabilities of specific engine designs during combustion. Findings showed that *ORCA* yielded predictions for coolant temperature and pressure drop of less than 5% discrepancy from alternative design tools.

The development of an easy-to-use user interface will streamline and accelerate engine design. The *ORCA* program as a whole is capable of far more than thermal and structural analysis, allowing the user to complete end-to-end engine design, with capabilities to design various injector types, as well as complete nozzle design.

V. Future Work

As this paper was developed as part of a Master's thesis constricted to a six-month timeline, several capabilities ideally would have been incorporated into *ORCA* but were deemed excessive of the time frame. The *ORCA* thermal analysis code will likely be improved in the coming years by the propulsion team within Glasgow University Rocketry, incorporating the following design features.

- Film Cooling - Film cooling is a common method of cooling the chamber wall, however, can be difficult to model. The addition of film cooling will greatly benefit the *ORCA* program, and will likely be completed as part of a future thesis.
- In its current state, *ORCA* does not account for temperature-dependent wall properties such as thermal conductivity. Although not as crucial as the temperature-dependent flow properties, the wall properties should ideally also vary with temperature, which can easily be added to the *MATLAB* code in future.
- Being able to dilute the coolant flow with water will be an important design aspect for many rocket engines intended for hot-fire static testing as this can greatly increase the specific heat capacity of the coolant flow. This too will likely be incorporated into *ORCA* in the coming years.
- Currently, *ORCA* is not set up for user inputs of variable channel height, a singular input is recorded for a constant channel height. Future development in *ORCA* would allow the user to input varying channel heights at varying engine locations.
- The ability to assess the predicted wall temperature at many locations within a cooling channel will provide the

user with a greater understanding of the engine design. For example, predicting temperatures at different locations within the wall, such as within the fin structure.

- *MATLAB* has integrated AI tools that could be incorporated into the *ORCA* heat transfer module, allowing machine learning to be used to optimise the design of the cooling channels. Rather than simply iterating through different designs and highlighting which produces the lowest wall temperatures, a trained AI model would test channel geometries in a streamlined fashion to obtain an optimized design over a shorter period.
- Due to the slight offset in accuracy *ORCA* has in comparison with alternative tools such as *COMSOL*, adapting the program to include correction factors will likely improve the accuracy of the output results. The Bartz equation commonly has correction factors applied for specific engine designs, a full study will be required to investigate the use of such correction factors, and whether or not they would apply irrespective of engine design or size.
- To be able to compare and validate the predictions of the *ORCA* program in comparison with recorded values from physical testing would be a highly beneficial step in the development of the program. This would be a key step towards applying correction factors, providing certainty in where *ORCA* is of greatest accuracy.

VI. Appendix

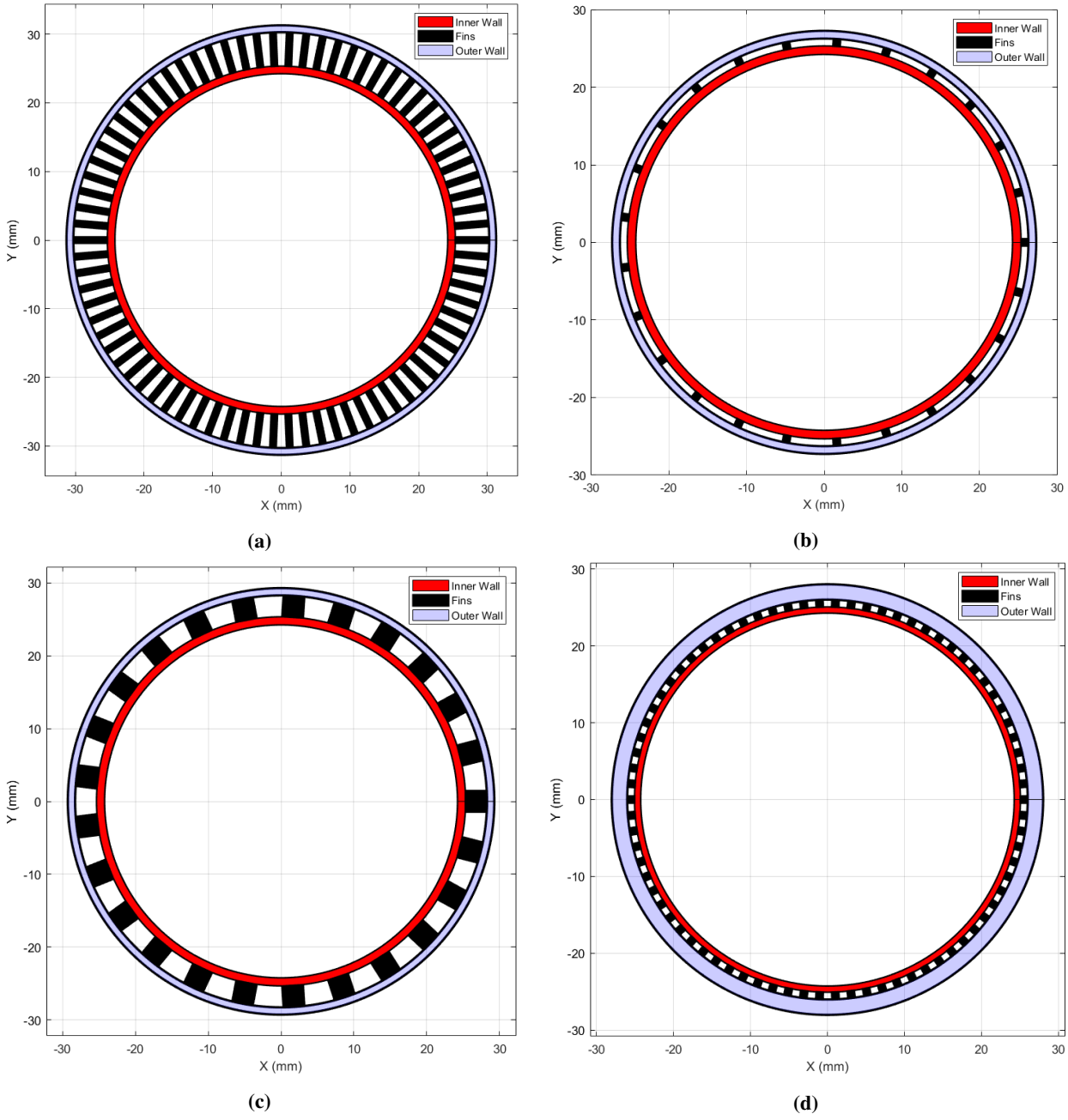

Fig. 15 Cross sectional view of cooling channel geometries designed for (a), high aspect ratio, (b), low aspect ratio, (C), large cross sectional area, and (d), the geometry outlined in Table 1.

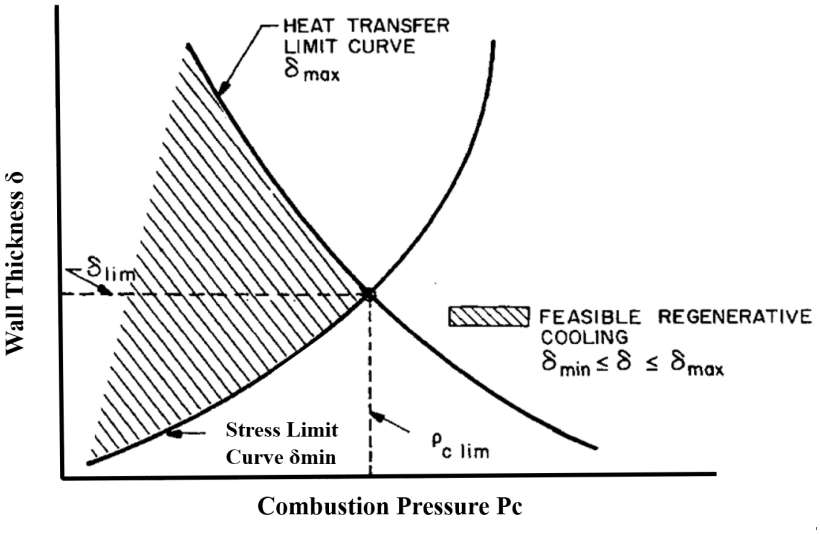

Fig. 16 Diagram depicting the wall thickness and combustion pressure bounds for stress limits due to pressure and thermal stresses, respectively [28].

Parameter	Value	Unit
Thrust	5000	N
Chamber Pressure	20	bar
Nozzle Expansion Pressure	1	bar
Coolant Inlet Pressure	25	bar
Characteristic Length	0.5	m
Total Mass Flow Rate	2.98	kg/s
Fuel and Oxidiser Inlet Temperature	300	K
Nozzle Half Angle	15	Degrees
Wall Thickness	0.7	mm
Outer Wall Thickness	2	mm
Channel height	1	mm
Channel width at chamber	2.735	mm
Channel width at throat	1.014	mm
Channel width at nozzle exit	2.735	mm
Fin width (constant)	1	mm
O/F Ratio	2	–
Contraction Ratio	5	–
Coolant Mass Flow Relative to Chamber	0.333	–
Nozzle Type	Conical	–
Fuel	Isopropyl Alcohol	–
Oxidiser	Nitrous Oxide	–
Wall Material	AlSi10Mg	–
Number of channels	78	–

Table 1 Design parameters for validation testing

References

[1] Kirchberger, C. U., "Investigation on Heat Transfer in Small Hydrocarbon Rocket Combustion Chambers," Ph.D. thesis, TECHNISCHE UNIVERSITÄT MÜNCHEN, 2014.

[2] Kose, Y. M., and Celik, M., "Regenerative Cooling Comparison of LOX/LCH4 and LOX/LC3H8 Rocket Engines Using the One-Dimensional Regenerative Cooling Modelling Tool ODREC," *Applied Sciences*, Vol. 14, No. 1, 2024. https://doi.org/10.3390/app14010071, URL https://www.mdpi.com/2076-3417/14/1/71.

[3] Bartz, D., "Technical Notes," *Journal of Jet Propulsion*, Vol. 27, 1957, pp. 49–53. https://doi.org/10.2514/8.12572.

[4] Huzel, D. K., *Modern Engineering for Design of Liquid-Propellant Rocket Engines*, AIAA, 1992.

[5] White, A., "Engine Cooling Design," , 2022. URL https://wikis.mit.edu/confluence/display/RocketTeam/Topic+5%3A+Engine+Cooling+Design.

[6] Chiu, H.-H., "RADIATION EFFECT ON ROCKET ENGINE PERFORMANCE," *NASA*, 1988. URL https://ntrs.nasa.gov/api/citations/19890012363/downloads/19890012363.pdf.

[7] White, A. J., "LS5: Engine Cooling Design," , 2022. URL https://wikis.mit.edu/confluence/display/RocketTeam/Topic+5%3A+Engine+Cooling+Design.

[8] Bills, J. D., "Overview of film cooling in a LRE," , 2016. URL https://api.semanticscholar.org/CorpusID:13946278.

[9] Richter, and Smith, "Ablative Material Testing for Low-Pressure, Low-Cost Rocket Engines," *NASA*, 1995. URL https://ntrs.nasa.gov/citations/19960007443.

[10] Beck, R. A. S., "Ablative Thermal Protection Systems Fundamentals," , 2017. URL https://ntrs.nasa.gov/api/citations/20170011453/downloads/20170011453.pdf.

[11] Reed, B., Biaglow, J., and Schneider, S., "ADVANCED MATERIALS FOR RADIATION-COOLED ROCKETS," *NASA*, 1993. URL https://ntrs.nasa.gov/citations/19940018579.

[12] Pederson, T., "A few micrometers of SiO2, please!" , 2018. URL https://copenhagensuborbitals.com/a-few-%CE%BCm-of-sio2-please/.

[13] Hyde, S., and Okninski, A., "Silicon Oil Thermal Barrier System for in Space Applications," , 05 2016. https://doi.org/10.13140/RG.2.1.2230.3601.

[14] Greuel, D., Suslov, D., Haidn, O., and Fritscher, K., "Thermal Barrier Coating for Cryogenic Rocket Engines," *38th AIAA/ASME/SAE/ASEE Joint Propulsion Conference and Exhibit*, Vol. 1, 2002. https://doi.org/10.2514/6.2002-4145.

[15] Gradl, P. R., "Channel Wall Nozzle Manufacturing Technology Advancements for Liquid Rocket Engines," *NASA*, 2019. URL https://ntrs.nasa.gov/citations/20190033314.

[16] Gradl, P. R., "Rapid Fabrication Techniques for Liquid Rocket Channel Wall Nozzles," *NASA*, 2016. URL https://ntrs.nasa.gov/api/citations/20160009709/downloads/20160009709.pdf.

[17] Kazaroff, J. M., and Pavli, A. J., "Advanced Tube-Bundle Rocket Thrust Chamber," *NASA*, 1990. URL https://ntrs.nasa.gov/citations/19900060172.

[18] Group, B. U. R. P., "Lotus Dev 2 Combustion Chamber," , 2024. URL http://heroicrelics.org/info/neosho/assy-line-produces-engines.html.

[19] Baker, N. L., "Assembly Line Produces Rocket Engines," , 2024. URL https://burpg.org/.

[20] Incropera, F. P., and Dewitt, D. P., *Introduction to heat transfer. Student solution manual*, Wiley ; Chichester, Hoboken, N.J., 2009.

[21] Ilic, M., Petrovic, M., and Stevanovic, V., "Boiling heat transfer modelling: A review and future Prospectus," *Thermal Science*, Vol. 2018, 2018, pp. 249–249. https://doi.org/10.2298/TSCI180725249I.

[22] P.H Kringe, M. O., J. R. Riccus, "LOW-COST LIFE ASSESSMENT OF LIQUID ROCKET ENGINES," , 2020. URL https://elib.dlr.de/138646/1/Kringe_2020_JBIS.pdf.

[23] Hötte, F., v. Sethe, C., Fiedler, T., Haupt, M. C., Haidn, O. J., and Rohdenburg, M., "Experimental lifetime study of regeneratively cooled rocket chamber walls," *International Journal of Fatigue*, Vol. 138, 2020, p. 105649. https://doi.org/10.1016/j.ijfatigue.2020.105649.

[24] Bai, Q., and Bai, Y., "9 - Thermal Expansion Design," *Subsea Pipeline Design, Analysis, and Installation*, edited by Q. Bai and Y. Bai, Gulf Professional Publishing, Boston, 2014, pp. 187–220. https://doi.org/https://doi.org/10.1016/B978-0-12-386888-6.00009-2, URL https://www.sciencedirect.com/science/article/pii/B9780123868886000092.

[25] SONG, J., and SUN, B., "Thermal-structural analysis of regeneratively-cooled thrust chamber wall in reusable LOX/Methane rocket engines," *Chinese Journal of Aeronautics*, Vol. 30, No. 3, 2017, pp. 1043–1053. https://doi.org/https://doi.org/10.1016/j.cja.2017.04.007, URL https://www.sciencedirect.com/science/article/pii/S1000936117301024.

[26] Hannuo, N. P., and Price, J., R. G., "Some effects of thermal-cycle-induced deformation in rocket thrust chambers," *NASA*, 1981. URL https://ntrs.nasa.gov/citations/19940018579.

[27] Waugh, I., Moore, E., Greig, A., Macfarlane, J., and Dick-Cleland, W., "ADDITIVE MANUFACTURE OF ROCKET ENGINE COMBUSTION CHAMBERS USING THE ABD-900AM NICKEL SUPERALLOY," , 2021. URL https://www.ael.co.uk/files/220_WAUGH.pdf.

[28] Pizzarelli, M., "Regenerative cooling of liquid rocket engine thrust chambers," , 11 2017. https://doi.org/10.13140/RG.2.2.30668.92804.

[29] Uzan, N. E., Shneck, R., Yeheskel, O., and Frage, N., "High-temperature mechanical properties of AlSi10Mg specimens fabricated by additive manufacturing using selective laser melting technologies (AM-SLM)," *Additive Manufacturing*, Vol. 24, 2018, pp. 257–263. https://doi.org/https://doi.org/10.1016/j.addma.2018.09.033, URL https://www.sciencedirect.com/science/article/pii/S2214860418302148.

[30] Saha, H., "Rocket engine thrust chamber wall temperature distribution calculation and analysis," *NASA*, 1976. URL https://ntrs.nasa.gov/citations/19760019183.

[31] Halaand, S. E., "Simple and Explicit Formulas for the Friction Factor in Turbulent Pipe Flow," *Fluids Engineering*, Vol. 105, 1983, pp. 89–90. URL https://asmedigitalcollection.asme.org/fluidsengineering/article-abstract/105/1/89/408126/Simple-and-Explicit-Formulas-for-the-Friction.

[32] Wassgren, C., "Pipe Flows," , 2021. URL https://engineering.purdue.edu/~wassgren/teaching/ME30800/NotesAndReading/PipeFlows_Losses_Reading.pdf.

[33] Naraghi, M., and Foulon, M., "A Simple Approach for Thermal Analysis of Regenerative Cooling of Rocket Engines," , 01 2008. https://doi.org/10.1115/IMECE2008-67988.

[34] Heister, S. D., Anderson, W. E., Pourpoint, T. L., and Cassady, R. J., *Rocket Propulsion*, Cambridge Aerospace Series, Cambridge University Press, 2019.